Nanoscale

PAPER

Check for updates

Polysalt ligands achieve higher quantum yield and improved colloidal stability for CsPbBr₃ quantum dots†

Sisi Wang, [ID] [a] Liang Du,[a] Selin Donmez, [ID] [a] Yan Xin[b] and Hedi Mattoussi [ID] *[a]

Colloidal lead halide perovskite quantum dots (PQDs) are relatively new semiconductor nanocrystals with great potential for use in optoelectronic applications. They also present a set of new scientifically challenging fundamental problems to investigate and understand. One of them is to address the rather poor colloidal and structural stability of these materials under solution phase processing and/or transfer between solvents. In this contribution, we detail the synthesis of a new family of multi-coordinating, bromide-based polysalt ligands and test their ability to stabilize CsPbBr₃ nanocrystals in polar solutions. The ligands present multiple salt groups involving quaternary cations, namely ammonium and imidazolium as anchors for coordination onto PQD surfaces, along with several alkyl chains with varying chain length to promote solubilization in various conditions. The ligands provide a few key benefits including the ability to repair damaged surface sites, allow rapid ligand exchange and phase transfer, and preserve the crystalline structure and morphology of the nanocrystals. The polysalt-coated PQDs exhibit near unity PLQY and significantly enhanced colloidal stability in ethanol and methanol.

Introduction

Colloidal all-inorganic lead halide CsPbX₃ (X = Cl, Br, I) perovskite quantum dots, PQDs, have generated enormous interest in recent years.[1–4] That interest is motivated by some of their unique photophysical properties, such as tunable bandgap, high photoluminescence quantum yield (PLQY) and narrow emission profiles, all combined with easy to implement solution phase synthesis and processing.[5,6] These materials are very promising for use in optoelectronic applications, including solar cell technology,[7–10] light-emitting diodes (LED),[11–13] liquid crystal display (LCD),[14] photodetectors[15] and scintillators.[16] In addition, PQDs exhibit high tolerance to structural defects, as rather shallow energy traps characterize these materials, a property traced to the orbital composition of the energy bands calculated for lead halide perovskites.[2,17] However, a major hurdle that has inhibited implementation of those promising applications and slowed the in-depth characterization of these materials (structure, optical and electronic

properties) has been their rather limited colloidal and structural stability, compared to the more "conventional" colloidal quantum dots made of metal chalcogenide cores. Some of these problems emanate from the ionic nature of the core crystals, which yield low internal lattice energy, a highly dynamic ligand binding onto the nanocrystal surfaces and limited structural stability in polar solutions.[18,19]

In a typical growth reaction of colloidal perovskite nanocrystals, a combination of alkyl acid (oleic acid, OA) and alkyl base (oleylamine, OLA) are used to form the metal–organic precursors and eventually surface stabilize the as-grown NCs in nonpolar media.[5] Those ligands interact with the nanocrystals in the form of primary ammonium (OLA⁺, hard Lewis acid) and carboxylate (OA⁻, hard Lewis base) ion pairs, and they exhibit rather weak affinity to the NC surfaces, which result in high rate of ligand desorption and reduced colloidal stability.[19] Additionally, it has been suggested that proton transfer between oleate and oleylammonium ions (in solution) can neutralize the surface-bound oleylammonium species, further weakening ligand affinity to the PQD surfaces.[18–20] These factors make solution phase grown PQDs very sensitive to solvent polarity. For example, a few rounds of precipitation using a non-solvent can induce loss of structural integrity, colloidal instability, coupled with a drop of fluorescence.[21,22] This indicates that solution processing would increase the density of structural defects (mostly surface-located), often associated with the large surface-to-volume ratio of the nanocrystals and

[a]*Florida State University, Department of Chemistry and Biochemistry, 95 Chieftan Way, Tallahassee, FL 32306, USA. E-mail: mattoussi@chem.fsu.edu*
[b]*Florida State University, National High Magnetic Field Laboratory, 1800 E. Paul Dirac Drive, Tallahassee, Florida, 32310, USA*
†Electronic supplementary information (ESI) available: Additional information, materials, instrumentation, NMR spectra of several polysalt ligands, TEM data of certain polysalt-QDs, and colloidal stability tests. See DOI: 10.1039/d1nr04753a

rather poor electronic passivation provided by weakly binding native ligands.[21,23] Consequently, the nature of the surface coating chemistry applied to stabilize these materials plays an important role in every aspect of their behavior, including colloidal stability, photophysical characteristics, carrier transport properties and the ability to carry out solution processing of the nanocrystals into thin film devices.[24,25]

Several studies have attempted to address the above limitations by identifying novel coatings that exhibit higher binding affinity to the PQD surfaces and better electronic passivation of defect states. Kovalenko and co-workers introduced zwitterionic-containing molecules such as alkyl sulfobetaine or phosphocholine derivatives during the growth reaction, to alter the composition of the final nanocrystal coating.[26,27] They reported that this strategy yielded QDs with better colloidal and structural stability under high dilution conditions and anti-solvent washes. Other groups including Manna and co-workers, Sun and co-workers, and Zeng and co-workers have substituted OLA/OA with alky phosphonic acid or benzenesulfonic acid as surfactants during synthesis, and reported the growth of PQDs with enhanced PLQY and better stability under few rounds of purification or under diluted conditions.[28-31] This improvement was attributed to the higher affinity of phosphonate groups to Pb^{2+} surface ions. As an alternative strategy to introducing new surfactants during growth, Alivisatos' group and Samanta's group implemented post growth treatment of the PQDs as a means of improving PLQY and colloidal stability. Post-treatment of PQDs with inorganic salts, such as thiocyanate and tetrafluoroborate, or alkyl phosphonate, were used to passivate under-coordinated surface Pb^{2+} sites, resulting in better fluorescence properties.[32-34] Another actively explored idea involves the use of didodecyl ammonium bromide (DDAB) as surface passivating ligands, which were either introduced during preparation or applied post-growth to the PQDs.[13,22,35-46] Despite these successes, rather modest progress has been realized using these various small molecule ligands, due to both lingering weak binding and modest steric stabilization of the PQDs.

In this report, we probe the capacity of a set of multidentate polysalt ligands based on the quaternary ammonium or imidazolium bromide motifs to provide stable coating and simultaneously improve the PL emission of colloidal perovskite quantum dots. The ligand design exploits the highly efficient nucleophilic addition reaction between amine-bearing blocks (as nucleophiles) and succinic anhydride rings in a low molecular weight poly(isobutylene-*alt*-maleic anhydride), PIMA, copolymer.[47-50] The resulting compounds present several copies of either alkyl ammonium or imidazolium (as bromide salt groups) for electrostatic coordination onto the PQDs, along with multiple alkyl chains with varying length (C_8 or C_{18}) to ensure expanded affinity of the polysalt-ligated nanocrystals to organic solvents with varying properties. Ligand substitution of OLA/OA-capped $CsPbBr_3$ PQDs with these polysalts yields NCs with significant enhancement in the PLQY, preserved absorption profiles and much better colloidal stability in polar media. Nuclear magnetic resonance (NMR) is used

to track changes in the surface coatings, and prove that a complete ligand exchange is achieved. Dynamic light scattering (DLS) measurements show that homogenous dispersions that are free of aggregates characterize the PQD colloids. Powder X-ray diffraction (PXRD) combined with transmission electron microscopy (TEM) data confirm that the integrity of the crystal structure and nanocrystal shape are essentially unaffected by the ligand substitution. Last, the stability of the nanocrystals has been evaluated using anti-solvent solution processing, probing resistance of the PQDs to water and easy phase transfer to polar solvents, including ethanol and methanol, without altering the nanocrystal integrity or optical properties of the materials even after extended storage.

Results and discussion

Rationale

There is a consensus in the community that the documented rapid degradation of the as-grown lead halide-based PQDs is initiated by etching of the nanocrystal surfaces during incubation and processing. This etching is facilitated by the ionic nature of the QD cores, and it tends to alter the surface structure as well as the integrity of the nanocrystals. We thus reasoned that designing a high affinity protective coating that presents several halide salt groups per ligand would competitively displace the native labile cap of the nanocrystals and progressively repair damaged sites, by sharing the halide ions with the QD surfaces. This would also improve the fluorescence quantum yields of the compounds.[33] Synthesis of the polysalts exploits the efficiency of the nucleophilic addition reaction between distinct amine-R nucleophiles and poly(isobutylene-*alt*-maleic anhydride) block copolymer, to design several high affinity coordinating ligands that are ideally adapted for stabilizing luminescent chalcogenide quantum dots and other transition metal nanoparticles.[47-49,51,52] Here, we use quaternary ammonium bromide or imidazolium bromide salts as coordinating groups onto PQD surfaces and alkyl chains to promote solubility in various organic media. Fig. 1A summarizes the general synthetic strategy for preparing our polysalts, where two steps are involved. Two distinct nucleophile precursors are combined for each set of ligands, namely *N,N*-dimethylaminopropylamine (AM) or 1-(3-aminopropyl)imidazole (IM) is used as salt source, while octylamine (OCA) or octadecylamine (ODA) provides the solubilizing alkyl chains. In a typical reaction, AM or IM is mixed with a PIMA solution in DMF. Then, OCA in DMF or ODA pre-dissolved in $CHCl_3$ is added to the mixture, which was pre-heated to ~60 °C, and left to react overnight while stirring. Then, the tertiary amine or imidazole groups are transformed into quaternary ammonium (AMB) or imidazolium (IMB) salts by reaction with bromoethane. The final products display several salt groups installed randomly along the polymer backbone (as schematically depicted in Fig. 1). Taking advantage of the versatility of this strategy, we synthesized six sets of polysalts with well-defined stoichiometry. Three ligands present AMB groups:
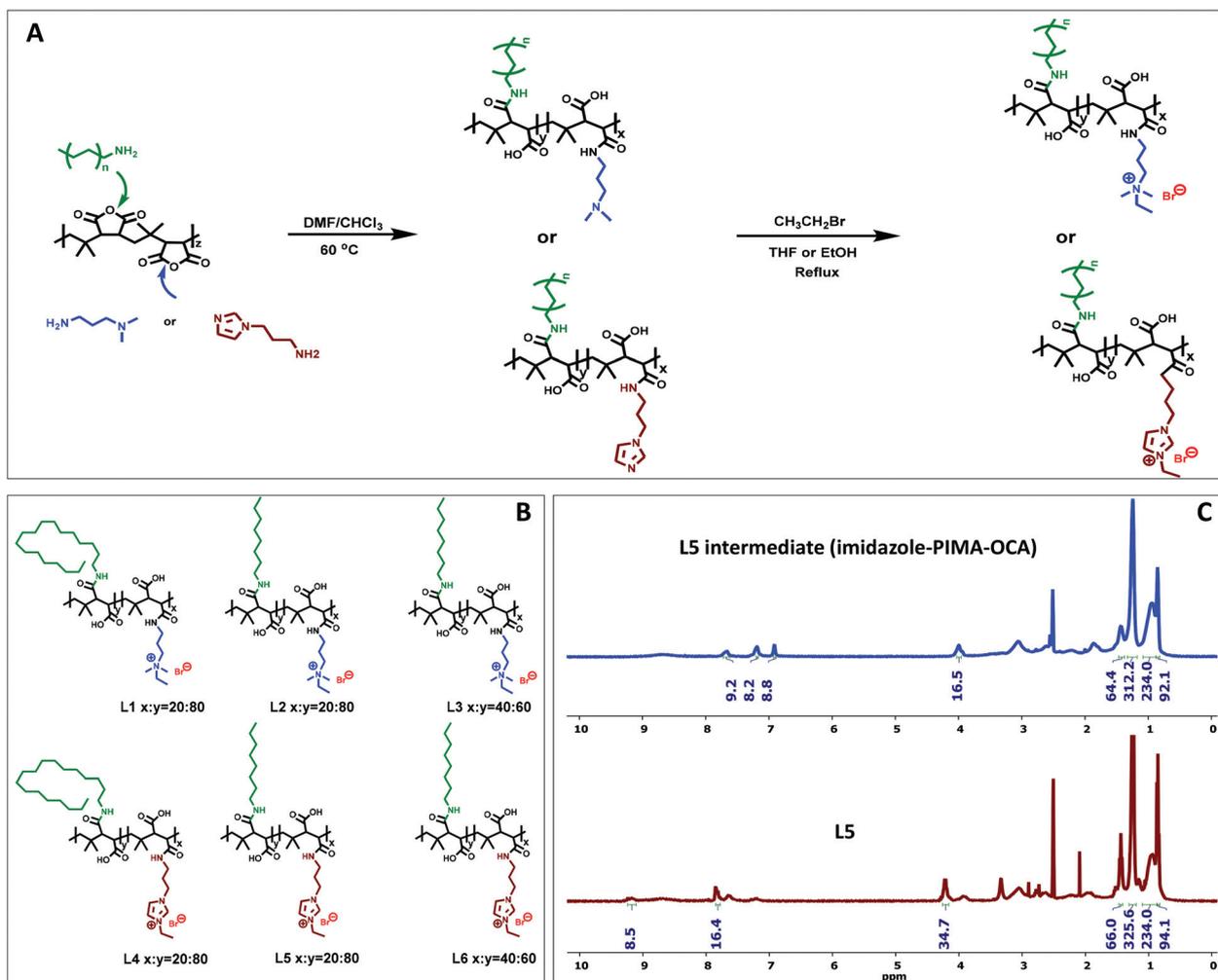
Fig. 1 (A) Schematic representation of the nucleophilic addition reaction used to prepare the polysalt ligands. (B) Structures and nomenclature of the ligands prepared and tested in this study. (C) ^{1}H NMR spectra collected from imidazole−PIMA−OCA (intermediate, top) and the corresponding imidazolium−PIMA−OCA polysalt **L5** (bottom). Both compounds were dissolved in DMSO-d$_6$.

L1 (AMB : ODA = 20 : 80); **L2**: (AMB : OCA = 20 : 80); **L3**: (AMB : OCA = 40 : 60); and three present IMB groups: **L4** (IMB : ODA = 20 : 80); **L5** (IMB : OCA = 20 : 80); **L6** (IMB : OCA = 40 : 60), see Table 1 and Fig. 1. Here, x and y designate the molar fraction of anchoring groups and solubilizing chains estimated with respect to the monomer concentration of the PIMA (there are ∼40 monomers per chain). As an example, synthesis of **L1** was carried out by reacting PIMA with a mixture of N,N-dimethylaminopropylamine and octadecylamine at 20 : 80 molar ratio, then followed by quaternization reaction alkylating the tertiary amine into alkyl ammonium bromide (AMB). Conversely, synthesis of ligand **L6** was carried out by reacting PIMA with 1-(3-aminopropyl)imidazole and octylamine at a molar ratio 40 : 60, and then transforming the imidazole into imidazolium bromide (IMB) in the presence of bromoethane. Further details about the synthetic steps are provided in the ESI.† The ^{1}H NMR data shown in Fig. 1 and ESI (Fig. S1–S3†) confirm the successful preparation of the various ligands with the desired structures. For instance, the spectra

acquired for IMB–PIMA–OCA show peaks at ∼9.2 ppm and ∼7.9 ppm characteristic of the imidazolium protons, while the peaks at ∼0.85 ppm and ∼1.24 ppm are respectively ascribed to the terminal –CH$_3$ and –CH$_2$ groups of octylamine. In addition, a broad peak centered at ∼0.95 ppm ascribed to the methyl protons along the polymer backbone is also measured. The degree of grafting is estimated by comparing the integration values of the ^{1}H NMR peaks of different moieties; details are listed in Table 1. It should be noted that the salt-to-ODA molar ratio could not be determined with good accuracy, due to broadening of the peaks and a pronounced overlap between the signatures of the ODA and PIMA methyl protons in the NMR spectrum. Nevertheless, quantification of the number of anchors and OCA chains in the other polysalts is indicative of good agreement between the nominal and measured stoichiometry values for the synthesized compounds (see Table 1). This agrees with prior studies, which have shown that the addition reaction yields polymers with stoichiometry that is very close to that anticipated from the nominal values

Table 1 Summary of the various polysalt ligands synthesized and used for stabilizing the CsPbBr$_3$ PQDs. The relative molar fractions of the starting nucleophiles with respect to the PIMA monomers are compared side-by-side to the experimental values estimated from the ^{1}H NMR data

Ligand	Molar ratio	Nominal number per chain[a]	Experimental number per chain from NMR[b]
L1: AMB–PIMA–ODA[c]	$x:y = 20:80$	AMB: 8; ODA: 32	—
L2: AMB–PIMA–OCA	$x:y = 20:80$	AMB: 8; OCA: 32	AMB: ~8 OCA: ~31
L3: AMB–PIMA–OCA	$x:y = 40:60$	IMB: 16; OCA: 24	AMB: ~16 OCA: ~24
L4: IMB–PIMA–ODA[c]	$x:y = 20:80$	IMB: 8; ODA: 32	—
			IMB : ODA ~1 : 4
L5: IMB–PIMA–OCA	$x:y = 20:80$	IMB: 8; OCA: 32	IMB: ~9 OCA: ~31
L6: IAB–PIMA–OCA	$x:y = 40:60$	IMB: 16; OCA: 24	IMB: ~14 OCA: ~26

[a] The reported values were obtained from the molar concentration of the amine-modified precursors, compared to that of the monomers in PIMA. [b] The values were obtained by comparing the ^{1}H NMR peak integration of ammonium dimethyl ($\delta \sim 3$ ppm), imidazolium ($\delta \sim 9.2$ ppm) and OCA ($\delta \sim 0.85$ ppm) to the two methyl groups in the polymer backbone (~234 H, $\delta \sim 0.97$ ppm). Spectral deconvolution was applied to resolve the overlapping peaks in the range of 0.8–1 ppm and extract the integration values. [c] Note that we have not attempted to extract accurate stoichiometry data for L1: AMB–PIMA–ODA and L4: IMB–PIMA–ODA, due to the strong overlap between the signatures of the alkyl chains and the dimethyl groups in PIMA.

based on the molar concentrations of the nucleophile precursors.[49,52]

Ligand exchange and phase transfer

CsPbBr$_3$ nanocrystals, grown *via* the hot injection method using oleic acid and oleylamine ligands (OLA/OA-PQDs), were used for testing the ability of the polysalt ligands to achieve high binding affinity, repair defect sites and provide electronic passivation.[5] Considering the different solubility characteristics of the various polymer compounds, ligand exchange with ODA or OCA containing polymers was carried out following slightly different protocols. For AMB–PIMA–ODA (L1) and IMB–PIMA–ODA (L4), the ligands are not soluble in polar media such as ethanol and methanol; the PQD stock dispersions in hexane were thus mixed with the polymer pre-dissolved in toluene yielding a clear mixture, then sonicated for ~5 minutes. The nanocrystals were washed with excess ethanol, precipitated, then re-dispersed in toluene and stored until further use. Conversely, the polymers containing short alkyl chains, AMB–PIMA–OCA (L2, L3) and IMB–PIMA–OCA (L5, L6) exhibit good solubility in ethanol and methanol. Ligand exchange and phase transfer was thus carried out using either a homogeneous one phase reaction (route 1), or a heterogeneous two-phase reaction (route 2), see Fig. 2A. (1) In the one phase reaction, hydrophobic PQDs dispersed in hexane were mixed with a clear THF solution of the ligands L2 and L5 (containing 8 salt groups each) and sonicated for 3–5 minutes. The ligands containing 16 salt groups (*i.e.*, L3 and L6) were however not completely soluble in THF, but addition of EtOH (at ~EtOH : THF ~ 1 : 2) yielded a clear solution of those polymers. Mixing the OLA/OA-PQDs with either set of polysalts under these conditions allowed rapid ligand substitution, manifesting in a change in the nanocrystal solubility. This can be easily tested by adding excess hexane, which readily precipitates the PQDs, yielding a green pellet and a clear supernatant free of QD materials after centrifugation. After discarding the supernatant, the pellet was subjected to one or two more rounds of washing with ethyl acetate, then readily dispersed in EtOH or MeOH. (2) In the two-phase reac-

tion (route 2), the nonpolar phase (hexane) containing OLA/OA-PQDs was mixed with a solution of the polysalt in methanol, yielding a top layer of hexane containing the PQDs and a bottom layer of the polymer solution in methanol. Sonication of the vial for 3–5 minutes readily promoted the transfer of the QDs to the methanol phase, as shown in Fig. 2A (R2). Decanting the hexane layer yielded a clear dispersion of the polymer-stabilized PQDs in methanol. While both methods effectively allow the phase transfer of the nanocrystals to polar solvents, each route offers a few advantages. For instance, route 1 minimizes exposure of the nanocrystals to polar conditions prior to complete ligand substitution with the polymer, and thus yields slightly more homogenous PQDs. Conversely, the bi-phasic reaction allows visual tracking of the phase transfer, but tends to produce traces of aggregated materials which result from transient exposure of the native QDs to methanol prior to a complete ligand substitution. Nonetheless, the small fraction of formed aggregates can be easily removed by centrifugation for 3–4 minutes, leaving a homogeneous dispersion of PQDs in methanol (see Fig. 2A).

Characterization of the ligand substitution using NMR spectroscopy and dynamic light scattering

Effectiveness of the surface stabilization strategy is paramount to both extracting accurate data on how the new ligands affect the photophysical characteristics of the materials and for their potential integration into various devices. We characterized the completeness of the ligand substitution by tracking changes in the ^{1}H NMR spectra collected from PQD dispersions after coating with the polysalts, compared to a typical spectrum collected from a dispersion of as-grown nanocrystals. Fig. 2B shows a representative side-by-side comparison between the ^{1}H NMR spectrum collected from OLA/OA-PQDs (top spectrum) and those measured from dispersions of nanocrystals stabilized with two IMB-based polysalt ligands, L4 (IMB–PIMA–ODA)-PQDs and L5(IMB–PIMA–OCA)-PQDs, see middle and bottom spectra. The polymer-coated samples have been subjected to two rounds of purification then dispersed in CDCl$_3$, while the dispersions of native PQDs have been sub-
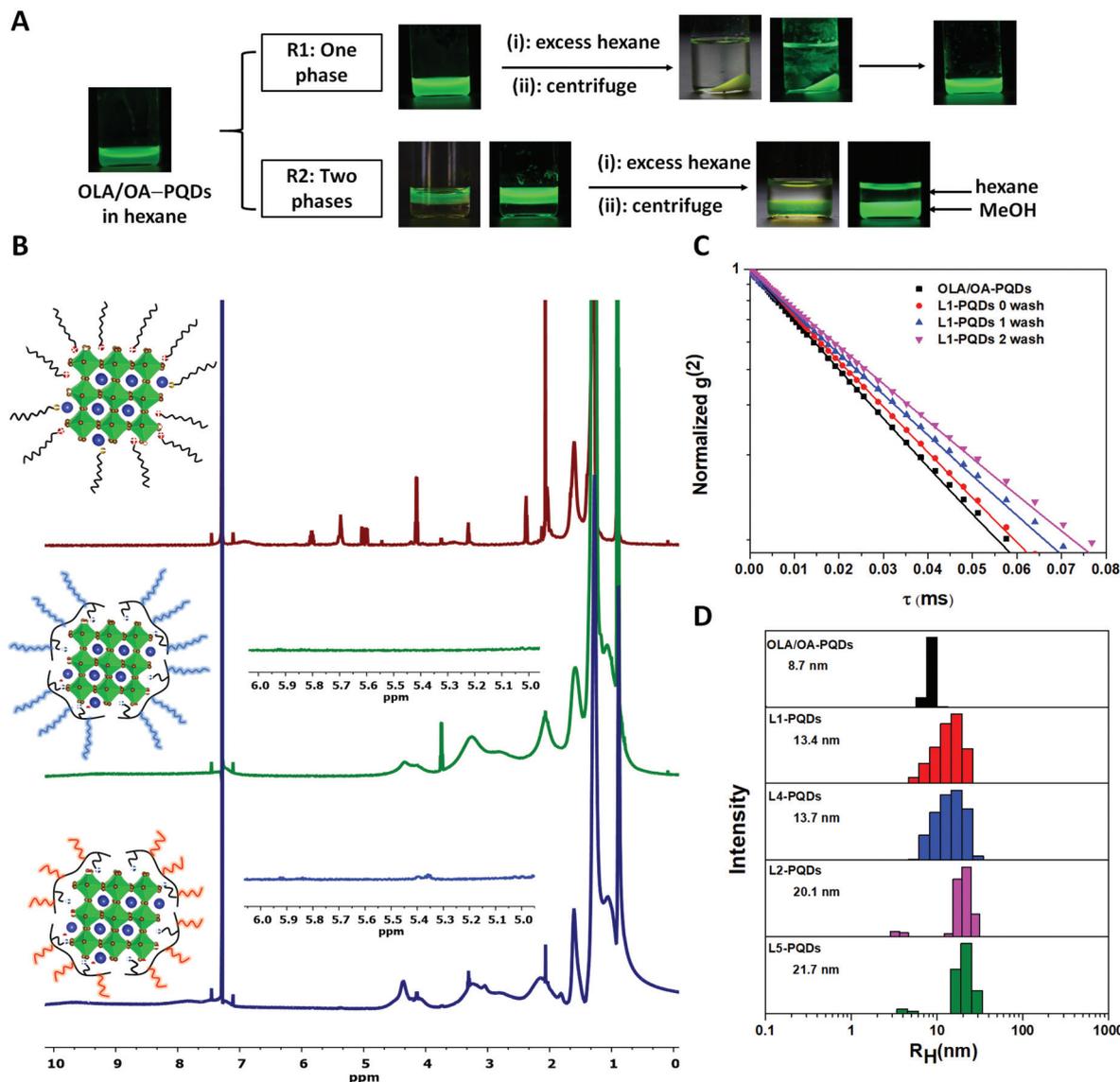
Fig. 2 (A) Fluorescent images (generated using a hand-held UV lamp, λ_{exc} = 365 nm) of PQDs collected during the ligand exchange steps with the polysalt ligands. One phase and two-phase routes are shown. (B) ^{1}H NMR spectra of PQDs coated with OLA/OA, IMB–PIMA–ODA (**L4**) and IMB–PIMA–OCA (**L5**) ligands; the PQDs were dispersed in CDCl$_3$. (C) Semi-logarithmic plot of the normalized intensity autocorrelation function ($g^{(2)}$) *vs.* τ recorded for PQD dispersions before, right after mixing with AMB–PIMA–ODA (**L1**) and after one time and two times washing with EtOH. (D) Histogram of hydrodynamic size distribution extracted from the Laplace transform of the autocorrelation functions built using the scattering data generated from the various PQD dispersions.

jected to only one cycle. The spectrum of the native PQDs shows signatures ascribed to oleate and oleylammonium protons in the 3–6 ppm range, in particular the alkene peak at 5.37 ppm, which is in good agreement with previous reports.[19,20,50] After ligand exchange with **L4** and **L5**, the spectra show several peaks spanning the range of 0–2 ppm, which are ascribed to the lateral alkyl chains and dimethyl protons along the PIMA backbone. Additionally, these spectra show broad peaks at ~4.3 ppm, which can be ascribed to the two ethylene –CH$_2$– directly attached to the imidazolium ring (N$_3$ position). Moreover, the characteristic downfield peaks of the imidazolium ring protons are not clearly discernable in

both spectra, presumably due to signal reduction and peak broadening, which can be attributed to two factors: a drastically reduced segmental mobility of the surface-coordinated imidazolium groups and a rather poor ligand solvation in CDCl$_3$.[53,54] Despite the ambiguity caused by the pronounced signal overlap in the upfield region (where the alkyl signatures are), the absence of signatures in the 5–6 ppm provides a solid proof for the complete removal of the native ligands from the polysalt-stabilized PQD samples (compare top spectrum to the middle and bottom spectra).[50]

Another test focused on verifying that the polysalt coating provides ample steric stabilization to the PQD nanocolloids, in

addition to enhancing PL. We applied dynamic light scattering (DLS) measurements to extract estimate of the hydrodynamic size and verify the homogeneity of the PQD colloidal dispersions. A plot of the autocorrelation function of the scattered intensity, $g^{(2)}(\theta, \tau)$ *vs.* τ (in semi-logarithmic scale) acquired from a dispersion of OLA/OA-PQDs shortly after mixing with excess IMB–PIMA–ODA (**L4**) shows that a slightly slower decay profile is acquired from the DLS data (see Fig. 2C). This accounts for a slight reduction in the Brownian diffusion of the nanocolloids compared to OLA/OA-PQDs, and reflects that a rapid adsorption of the polymer ligands onto the NCs has taken place. Applying one or two rounds of washing with ethanol further reduces the decay slope of the nanocolloids, resulting from the complete removal of the native ligands and their substitution with the polysalt, until equilibrium conditions are reached. Fig. 2D shows a set of intensity *vs.* hydrodynamic size histograms measured for dispersions of OLA/OA- and AMB/IMB–PIMA–ODA-PQDs in toluene and AMB/IMB–PIMA–OCA-PQDs in EtOH; these were extracted from the Laplace Transform of $g^{(2)}$ *vs.* τ profiles.[55] A single population is measured for all the samples, indicating that the PQD dispersions, before and after ligand substitution, are homogeneous and free of aggregates. Data also indicate that the smallest size is measured for the native coating, $R_{\mathrm{H}} \sim 8.7$ nm, then the size slightly increased to R_{H} (**L1**- and **L4**-PQDs in toluene) $\sim$ 13–14 nm and R_{H} (**L2**- and **L5**-PQDs in EtOH) $\sim$ 20–22 nm. These slight variations reflect differences in the hydrodynamic contributions of the coating to the Brownian diffusion of PQDs. More precisely, the larger size of the polysalts compared to the native OLA/OA yields higher contribution of the hydrodynamic interactions to the measured R_{H} compared to that measured for the as-grown materials.

Optical characterization

Having established the ability of the polysalts to rapidly promote ligand exchange and phase transfer of the PQDs, we proceed to characterize the optical properties of the resulting materials. More precisely, we first compare side-by-side the absorption and photoluminescence spectra collected from the PQDs coated with the various AMB- and IMB–PIMA–OCA ligands (*e.g.*, **L2** and **L5**) dispersed in EtOH to those measured for OLA/OA-PQDs in hexane, see Fig. 3A. There is a close match between the absorption profiles of both sets of materials, clearly indicating a retention of the nanocrystal integrity after ligand substitution. The PL intensity of the polysalt-capped samples is enhanced by 1.5 times, compared to the starting PQDs. The corresponding average PL lifetimes, extracted for the time-resolved decay profiles shown in Fig. 3B, are also longer than those measured for the as-grown materials, indicating reduction in the number of nonradiative channels (*i.e.* surface trap states) by the polysalt coating. Indeed, near-unity absolute PLQY ($\geq$95%) is measured for both AMB–PIMA–OCA (**L2**, **L3**)- and IMB–PIMA–OCA (**L5**, **L6**)-coated samples, compared to PLQY of $\sim$65% for OLA/OA-PQDs. Similar effects have also been measured for the PQDs ligand substituted with AMB–PIMA–ODA and IMB–

PIMA–ODA (**L1** and **L4**) and dispersed in toluene, namely fully preserved optical absorption and emission profiles and near unity PLQY, see Fig. 3C and D. The consistency of the results obtained for all polysalt (**L1–L6**)-stabilized CsPbBr$_3$ nanocrystals proves the importance of the salt groups for providing higher degree of surface passivation than OLA/OA and rules out potential additional effects of size or number of the solubilizing alkyl chains used. The lifetime data are compared to the changes in the ensemble fluorescence intensity using the relation for the PLQY:[56]

$$\mathrm{PLQY} = \frac{k_{\mathrm{r}}}{k_{\mathrm{r}} + k_{\mathrm{nr}}} \quad (1)$$

where k_{r} and k_{nr} respectively designate the radiative and nonradiative decay rates. Assuming that only k_{nr} is altered by electronic passivation of the surface traps, we compare the changes in the PLQY deduced from the ensemble PL to those extracted from changes in the lifetime data:

$$\frac{\mathrm{PL}_{\mathrm{polysalt}}}{\mathrm{PL}_{\mathrm{native}}} = \frac{\mathrm{PLQY}_{\mathrm{polysalt}}}{\mathrm{PLQY}_{\mathrm{native}}} = \frac{k_{\mathrm{r\text{-}native}} + k_{\mathrm{nr\text{-}native}}}{k_{\mathrm{r\text{-}polysalt}} + k_{\mathrm{nr\text{-}polysalt}}} = \frac{\tau_{\mathrm{polysalt}}}{\tau_{\mathrm{native}}} \quad (2)$$

where we replaced $\frac{1}{k_{\mathrm{r}} + k_{\mathrm{nr}}}$ with the PL lifetime, τ, extracted from the experimental data. From the steady-state and time-resolved data, estimates of the changes in the PLQY are compared to changes in the lifetime (see Table 2). Data show that the ratios between the PLQYs and PL lifetimes measured before after ligand substitution are consistently higher than 1 for both sets of polysalts, implying that the ligands improve the fluorescence properties of the nanocrystals. Nonetheless, the ratios extracted for the PL are slightly higher than those deduced from the lifetime data. For example, for the IMB-presenting polysalt, we find that:

$$\frac{\mathrm{PL}_{\mathrm{polysalt\text{-}IMB}}}{\mathrm{PL}_{\mathrm{native}}} \sim 1.62, \text{ or } 1.55$$

$$\frac{\tau_{\mathrm{polysalt\text{-}IMB}}}{\tau_{\mathrm{native}}} \sim 1.27 \text{ or } 1.34 \, (\text{for ODA and OCA}).$$

Characterization of the crystal structure and morphology of the PQD colloids

We first carried out powder X-ray diffraction (PXRD) experiments to identify the crystalline structure of the PQDs before and after stabilization with the different polysalt coatings. Fig. 4A shows the PXRD patterns acquired from the native OLA/OA-PQDs along with those ligand-exchanged with the set of polysalt ligands (**L1**, **L2**, **L4**, **L5**). Close inspection of the patterns reveals highly crystallized orthorhombic (*Pnma*) perovskite phase for all samples, confirmed by the close matching with the pattern measured for the bulk perovskite standard (ICSD number 243735).[57–59] We note that in our previous report,[50] we fitted the PXRD patterns to a cubic structure. However, given the close patterns measured for the cubic and orthorhombic phases and recent progress in the literature, we have now compared our XRD data to orthorhombic crystal structure.[59] The above result combined with absence of any "impurity peaks" from those spectra clearly indicate preserved
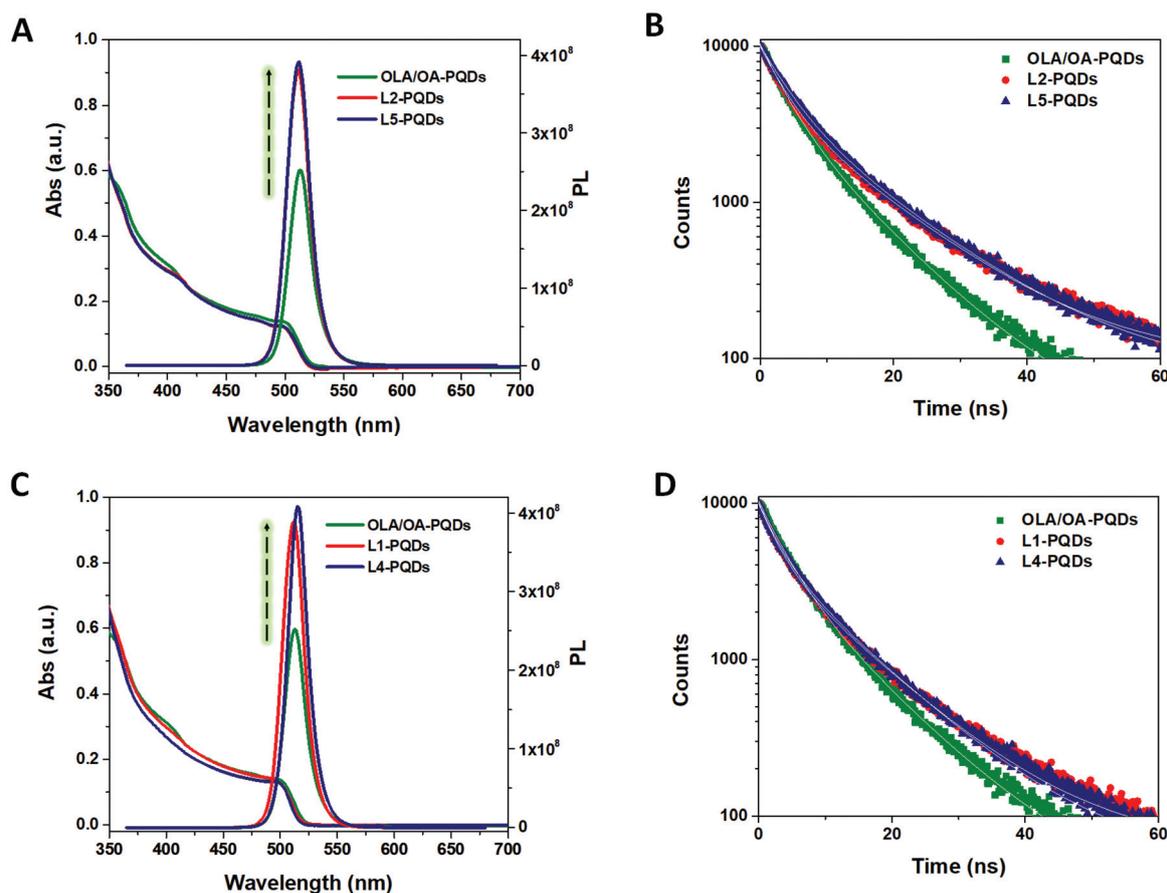
Fig. 3 (A) Absorption and fluorescence spectra of OLA/OA-PQDs in hexane along with AMB−PIMA−ODA (**L2**)-PQDs and IMB−PIMA−ODA (**L5**)-PQDs dispersed in EtOH. (B) The time-resolved PL decay profiles of the three sets of PQDs shown in A. (C) Absorption and fluorescence spectra collected from dispersions of OLA/OA-PQDs in hexane, **L1**-PQDs and **L4**-PQDs dispersed in toluene. (D) The time-resolved PL decay profiles of the three sets of PQDs shown in C.

Table 2 PL lifetime and PLQY acquired from dispersions of PQDs with different coatings. The lifetime values are reported together with the lifetime ratios measured for the polysalt- and OLA/OA-PQDs

PQDs	Lifetime, τ	Lifetime ratio	PLQY	$PL_{normalized}$
OLA/OA-PQDs	7.9 ns	1	~65%	1
L1-PQDs	8.8 ns	1.11	~90%	1.55
L4-PQDs	10.0 ns	1.27	~95%	1.62
L2-PQDs	10.4 ns	1.32	~94%	1.51
L5-PQDs	10.6 ns	1.34	~98%	1.55

crystal structure of the PQDs after ligand substitution with the polysalts. We then used high-angle-annular-dark-field scanning transmission electron microscopy (HAADF-STEM) to gain information about the spacing between the crystal planes, morphology and size distribution of the polysalt-stabilized PQDs, compared to the native OLA/OA-capped NCs. We focus on the TEM images acquired from nanocrystals ligated with **L2** (AMB20%−PIMA−OCA) and **L5** (IMB20%−PIMA−OCA) which allow phase transfer of PQDs to polar media, providing a more convincing proof that those poly-

mers preserve the integrity of the nanocrystal characteristic features under polar solution conditions (namely, size, shape and crystal structure). In order to examine whether or not possible changes in the core shape and size can take place during long-term storage, **L2**- and **L5**-stabilized PQDs dispersed in EtOH were first aged for ~3 months before acquiring the HAADF-STEM images. Freshly prepared OLA/OA-PQDs with cuboidal shape, sharp edges, and an average cube side length of ~7.2 nm were used as a reference, see Fig. 4, panel B. The image shown in Fig. 4, panel C indicates that **L2**-stablized PQDs prepared from dispersion in EtOH maintain their cubic shape with an average side length of ~7.4 nm. This proves that following ligand substitution the NPs preserve their overall size, shape, and stay homogenous and free of aggregates, albeit with a slightly broader size distribution (compare Fig. 4B and C). Nonetheless, PQDs ligand exchanged with **L5** (IMB20%−PIMA−OCA) exhibit more pronounced morphology changes. Though a cuboidal shape for the **L5**-PQDs can still be identified in the TEM image, a loss of corner sharpness and occasional etching of the nanocrystals is observed at higher magnification of individual nano-
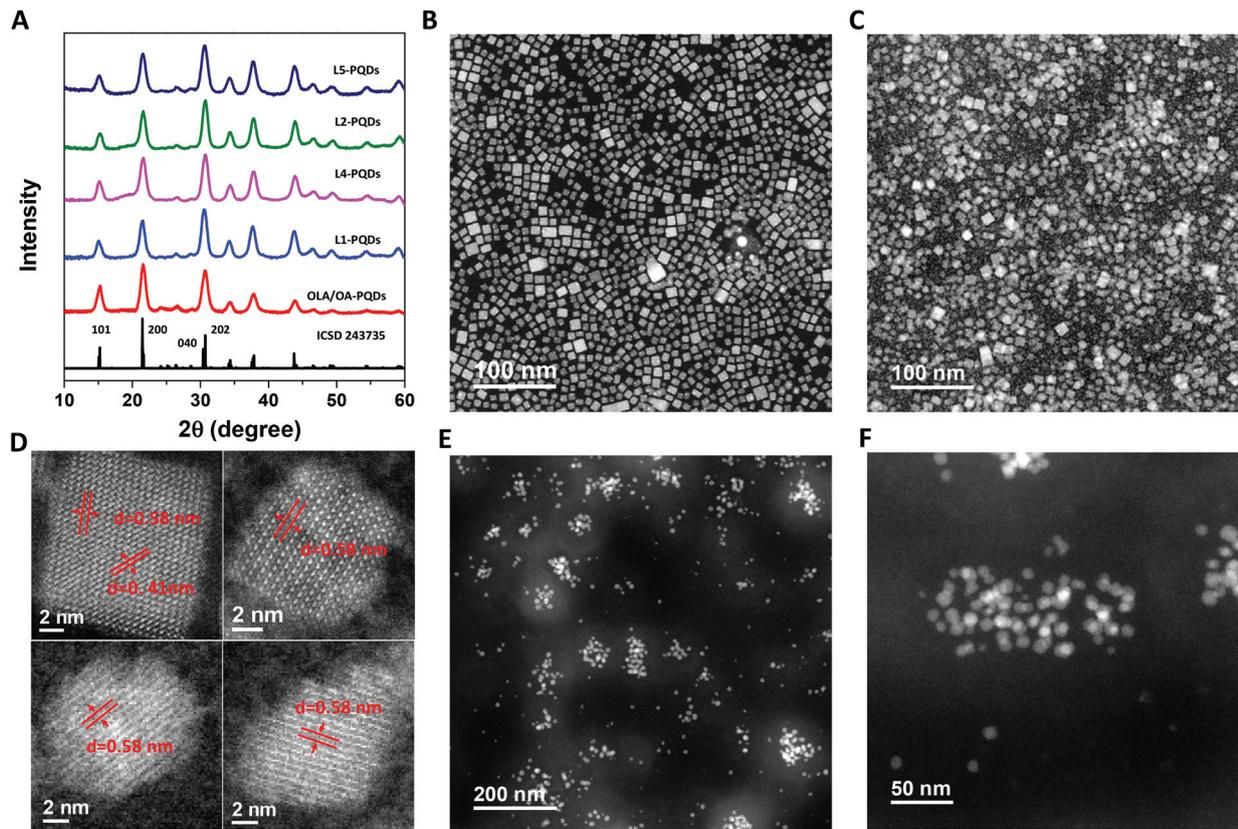
Fig. 4 (A) Powder XRD patterns of the native PQDs along with nanocrystals ligand exchanged with various polysalts. (B and C) HAADF–STEM images of OLA/OA-PQDs and AMB20%–PIMA–OCA-PQDs (**L2**). (D) Representative high resolution TEM images of single perovskite nanocrystals acquired from: OLA/OA-PQDs (top left); **L2**(AMB20%–PIMA–OCA)-PQDs (top right); **L5**(IMB20%–PIMA–OCA)-PQDs (bottom left and bottom right). (E and F) Lower magnification HAADF–STEM images of **L5**(IMB20%–PIMA–OCA)-PQDs. All polysalt-coated PQDs have been aged in EtOH for ~3 months prior to TEM measurements.

crystals (see Fig. 4D, bottom images). An average side length of ~7.5 nm is measured for these nanocrystals. Additional histograms on the PQD size distribution for the characterized samples are provided in the ESI, Fig. S4.† Cumulatively, the data show that essentially small to negligible changes in the core size are noted for the polymer-coated PQDs, indicating that minimal morphological transformation of the nanocrystals has taken place. The TEM images acquired from all three sets of samples show high core crystallinity with well-resolved atomic arrangements, where the spacing between the (101) crystal planes is ~0.58 nm and that between the (200) planes is ~0.41 nm (see panel 4D). Overall, we find that **L2**-PQDs have preserved their cubic morphology, while **L5**-PQDs show more visible corner etching, which can be identified under crystal orientation (see Fig. 4D, bottom images).[60,61] Interestingly, the PLQY measured for dispersion of all PQD samples after ligand substitution remained high. These findings indicate that the etching observed for some of the nanocrystal surfaces do not negatively affect the fluorescence properties of the materials. We attribute this to a more effective passivation of the surface defects brought by the multi-coordination of the nanocrystals after ligand substitution.

This reduces the overall rate of non-radiative exciton recombination for these dispersions.

Finally, we would like to note that even though the TEM images show rather homogenously distributed nanocrystals on the grid for OLA/OA-PQDs and **L2**-PQDs, the images collected from the **L5**-PQDs indicate that some degree of nanocrystal clustering, within discrete regions, builds up during the drying process, see low magnification images in Fig. 4E and F and Fig. S5.† We attribute this to inhomogeneous drying of the polymer-ligated PQDs on the TEM grid, a process likely due to the nature of the IMB–PIMA–OCA ligand and its affinity to EtOH.

Stability tests

We now proceed to evaluate the colloidal stability of the surface-modified PQDs under a few relevant testing conditions.

1- We first implement the ubiquitous polar solvent wash test (*e.g.*, ethanol or ethyl acetate). This method has been widely used for testing the new ligand affinity to the PQDs.[21,26,30] Additionally, washing with a polar solvent is a common technique for removing free OLA/OA ligands from

the medium, which is critical for integration into opto-electronic devices and improving the device efficiency.[35,38] Here, we compare the behaviors of OLA/OA-PQDs and polysalt-PQDs subjected to such treatment. We find that one wash of OLA/OA-PQDs with ethanol promote a rapid formation of a yellowish macroscopic aggregate and pronounced loss of emission, as shown in Fig. 5A. In contrast, dispersions of PQDs stabilized with **L1** (AMB–PIMA–ODA) or with **L4** (IMB–PIMA–ODA) preserve their colloidal integrity and strong emission properties, even when subjected to as many as five rounds of washing with ethanol, as reflected by the clear green fluorescent dispersions shown in Fig. 5A. Interestingly, the graph shown in Fig. 5B indicates that the effects of implementing the ligand substitution on the PL changes are subtle. Following simple mixing of a dispersion of OLA/LOA-PQDs with the polysalt yields a modest increase in the PL intensity (~30%). However, applying one round of washing with ethanol produces a large PL increase (~80%); further washing with ethanol did not affect the PL increase. We attribute this result to the removal of the native OLA/OA ligands and the ability of the polysalts to repair defects sites, passivate energy traps and improve the materials colloidal stability.

2- We then evaluate the resistance of PQDs to water-induced degradation for the three sets of samples, OLA/OA-PQDs, **L1**- and **L4**-stablized PQDs, using a two-phase (organic/water) configuration.[62] As shown in Fig. 5C, two separate phases are formed after mixing the dispersions with water, with the top toluene phase containing the PQDs and DI water in the bottom phase, due to the immiscible nature of the two liquids. Nonetheless, interaction between the PQDs and water can still take place through the interfacial interactions at the meniscus, in part due to local mixing and non-negligible water dissolution in toluene; water solubility in toluene at ambient conditions is at ~0.027 M.[63] This has caused turbidity buildup in the OLA/OA-PQDs layer combined with loss of fluorescence emission after one day, as shown in the white light and fluorescence images collected from these nanocrystal dispersions. In contrast, **L1**- and **L4**-stabilized PQDs stay dispersed and strongly fluorescent over the 3-day test period.

3- We carried out long-term colloidal stability tests, which is a highly relevant criterion for evaluating the effectiveness of the polysalt ligands to coordinate and stabilize the nanocrystals in solution. We probe the homogeneity and PL stability of PQDs ligand substituted with **L2** and **L5**, or **L3** and **L6**, and dispersed in two polar protic alcohols (EtOH and MeOH). Fig. 5D, left panel shows the fluorescence images of PQDs dispersions freshly prepared and after several months of storage under room light and temperature conditions. The PQDs coated with **L2** or **L5** (presenting 8 AMB or 8 IMB groups per ligand) exhibit rather limited stability in MeOH, where aggregation and PL quenching occurred after 1 month of storage. Better stability is shown in ethanol where homogeneity of the dispersion and high fluorescence emission are preserved for at least 4 months. In comparison, the colloidal and photo-
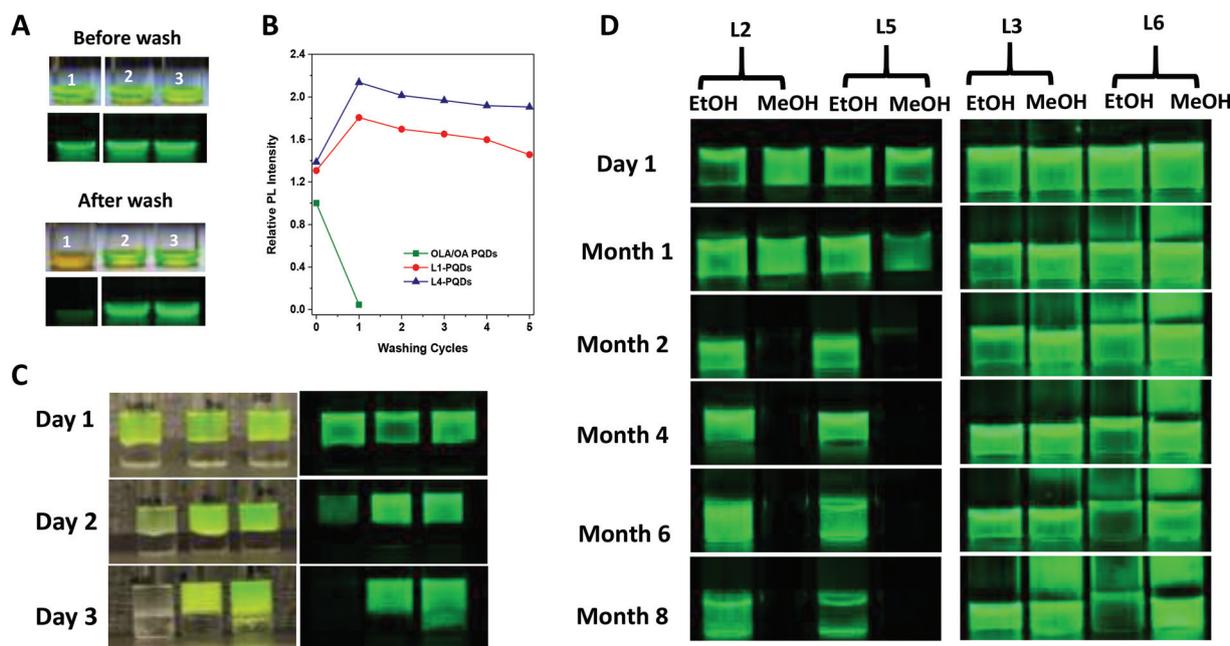

Fig. 5 (A) White light and fluorescence images acquired from dispersions of the native PQDs (1) before and after one EtOH wash, along with dispersions of **L1**-PQDs (2) and **L4**-PQDs (3), before and after 5 rounds of EtOH wash. (B) Plot of the relative PL intensity measured for pristine OLA/OA-PQDs, or **L1**-PQDs and **L4**-PQDs subjected to different EtOH wash cycles. (C) White light and fluorescence images acquired from OLA/OA-, **L1**- and **L4**-PQDs taken during the water resistance test; top layer is toluene and bottom layer is DI water. (D) Fluorescence images of AAB–PIMA–OCA (**L2** and **L3**)- and IAB–PIMA–OCA (**L5** and **L6**)-PQD dispersions in EtOH and MeOH tracked during storage for 8 months.

physical stability are much improved for PQDs that have been coated with ligands that present ~16 salt groups per chain (*i.e.*, **L3** and **L6**). As shown in Fig. 5D, panel 2, the 4 PQD samples stay homogeneous and highly fluorescent after 8 months of storage, a result that can be attributed to the stronger ligand affinity to the PQDs. Additionally, the absolute PLQY measured for the PQD dispersions in EtOH stay above 90% for at least three months (Fig. S6†). These findings agree with the reported benefits of using multi-coordinating ligands to impart long term structural and photophysical stability onto plasmonic and conventional luminescent nanocolloid materials.[64,65] Nonetheless, there are some subtle differences between ligands appended with ammonium and imidazolium salt groups. In general, we have found that AMB-based polymers (*e.g.*, **L2** and **L3**) impart better stability to NCs, which may likely be due to the smaller alkyl ammonium anchors compared to imidazolium rings. Fig. 5D and Fig. S7† show that **L2**-PQDs in ethanol maintain colloidal homogeneity and high PL for up to 6 months, while **L3**-PQDs stay stable for over one year of storage. This can be contrasted with IMB–PIMA–OCA-PQDs, which lose their colloidal stability and/or emission properties after ~4 months for **L5** and after ~8 months for **L6**.

We now discuss our findings in comparison to previous literature data and provide a few insights into how the polysalts combine strong coordination interactions and electronic passivation of the PQD surfaces. In particular, our comparison will focus on data collected from either treating the as grown $CsPbBr_3$ QDs with the molecular scale quaternary ammonium bromide, DDAB, or ligand substitution of the nanocrystals with these and other coordinating molecules. Those studies have overall reported that DDAB and other bromide salts can improve the photoemission properties of PQDs.[13,22,25] Nonetheless, monomer ligands applied to any colloidal nanocrystals tend to exhibit rather high rates of desorption due to the nature of coordination interactions.[66]

Our ligand design strategy to install several quaternary ammonium or imidazolium groups along a polymer backbone has promoted a substantial reduction in the rate of desorption, resulting in strengthened ligand interactions with the PQDs. This enabled a more efficient elimination of bromide vacancies (V_{Br}), better passivation of the Pb^{2+} sites, and filling the Cs^+ vacancies, thus restoring damaged lead-bromide octahedra near the NC surface (see Fig. 6). This has also improved the rate of exciton radiative recombination, ultimately increasing the measured PLQY to near unity, which is in agreement with data collected using monomeric DDAB.[22,67] Furthermore, multi-coordinating polymer ligands containing either ammonium or imidazolium cations would have more stable binding to the surface bromide ions, while promoting steric repulsions between individual PQDs brought by the multi-alkyl chains, compared to the monodentate DDAB ligands. This ultimately results in enhanced colloidal stability. We should also note that though some degree of surface etching of the NCs has been observed when using imidazolium-presenting polysalts, the absorption and PL spectra measured for those PQDs are unaffected. This indicates that slight damage of the nanocrystal surface does not significantly affect the photophysics of these materials, given their reported high tolerance to defects.[2,17] Finally, we would like to compare the present coating strategy results to those using polyzwitterionic ligands, described in references.[50,68,69] The two sets of ligands (polyzwitterion and polysalt) interact differently with the NC surfaces. While the polysalts can restore surface vacancies and removal of energy traps, their binding interaction are weaker than those afforded by the zwitterion-rich ligands. Polymer ligands based on the zwitterion motif(s) present two complementary coordinating groups (Lewis base and Lewis acid) which allow interactions with anionic and cationic sites on the PQDs, while a polysalt has only one set. This explains the better long term colloidal stability afforded by sulfobetaine-rich polymers such as those investigated in reference.[50]
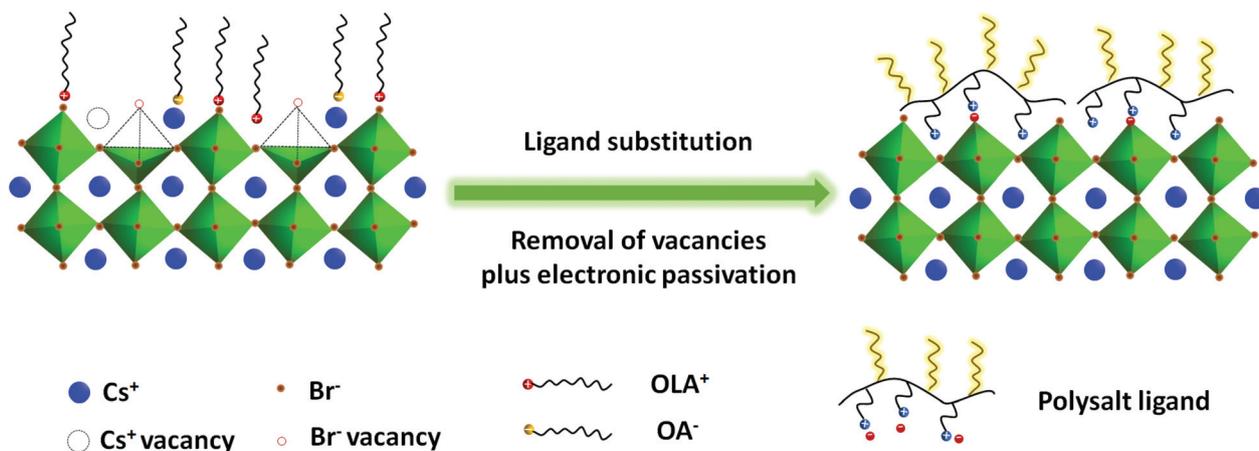

Fig. 6 Schematic representation of the benefits combining bromide vacancy filling and electrostatic passivation of the Cs^+ sites provided by the multidentate polysalt ligand coating, yielding enhanced PL and long-term colloidal stabilization of the PQDs.

Conclusion

We have designed and tested a set of polysalt compounds that combine several quaternary ammonium or imidazolium salt groups with multiple alkyl chains as high affinity coordinating ligands that promote colloidal stabilization while increasing the photoluminescence quantum yield of $CsPbBr_3$ PQDs. The salt groups and solubilizing alkyl chains were installed along a low molecular weight anhydride-rich copolymer using the nucleophilic addition reaction. We find that these polysalts provide rapid ligand substitution of the native coating, enhance the colloidal stability under various conditions (including extended storage in polar solutions, repeated washes with anti-solvents and exposure to water) and increase the PLQY to near unity, all without altering the crystalline structure or morphology of the nanocrystals. Complete removal of the native coating is confirmed using NMR spectroscopy.

We attribute the effectiveness of these ligands to the strong coordination interactions of the polysalts with the QD surfaces, and the ability of the ammonium or imidazolium bromide salt groups to provide two important features: (1) repairing of surface defect sites, by sharing the bromide anions with the nanocrystal surfaces; (2) filling the empty Cs^+ site with quaternary ammonium or imidazolium cations. These provide efficient electronic passivation of the surface energy traps, and in turn increase the exciton radiative recombination rate and enhance the PLQY of the dispersions to near unity. These results confirm the importance of combining high coordination with the specific salt structure for achieving increased ligand affinity to the nanocrystals while drastically reducing the rates of ligand desorption. This design can be used to develop other polysalt compounds that are optimized for other perovskite core stoichiometry. We are presently investigating the ability of these ligands to surface passivate and stabilize anisotropic $CsPbBr_3$ 2D nanoplates. We hope to report on these findings in the future. Other potential use of these rationales could involve the synthesis of additional halide (chloride or iodide) polysalts to promote better passivation of other core perovskite materials. Indeed, electronic passivation and structural stabilization of such materials is critical for further integration of these materials in a variety of optoelectronic applications.[70]

Conflicts of interest

There are no conflicts of interest to declare.

Acknowledgements

References

1 Q. A. Akkerman, G. Rainò, M. V. Kovalenko and L. Manna, Genesis, challenges and opportunities for colloidal lead halide perovskite nanocrystals, *Nat. Mater.*, 2018, **17**, 394–405.

2 M. V. Kovalenko, L. Protesescu and M. I. Bodnarchuk, Properties and potential optoelectronic applications of lead halide perovskite nanocrystals, *Science*, 2017, **358**, 745–750.

3 G. Almeida, I. Infante and L. Manna, Resurfacing halide perovskite nanocrystals, *Science*, 2019, **364**, 833–834.

4 J. Shamsi, A. S. Urban, M. Imran, L. De Trizio and L. Manna, Metal Halide Perovskite Nanocrystals: Synthesis, Post-Synthesis Modifications, and Their Optical Properties, *Chem. Rev.*, 2019, **119**, 3296–3348.

5 L. Protesescu, S. Yakunin, M. I. Bodnarchuk, F. Krieg, R. Caputo, C. H. Hendon, R. X. Yang, A. Walsh and M. V. Kovalenko, Nanocrystals of Cesium Lead Halide Perovskites (CsPbX3, X = Cl, Br, and I): Novel Optoelectronic Materials Showing Bright Emission with Wide Color Gamut, *Nano Lett.*, 2015, **15**, 3692–3696.

6 S. Wei, Y. Yang, X. Kang, L. Wang, L. Huang and D. Pan, Room-temperature and gram-scale synthesis of CsPbX3 (X = Cl, Br, I) perovskite nanocrystals with 50–85% photoluminescence quantum yields, *Chem. Commun.*, 2016, **52**, 7265–7268.

7 E. M. Sanehira, A. R. Marshall, J. A. Christians, S. P. Harvey, P. N. Ciesielski, L. M. Wheeler, P. Schulz, L. Y. Lin, M. C. Beard and J. M. Luther, Enhanced mobility $CsPbI_3$ quantum dot arrays for record-efficiency, high-voltage photovoltaic cells, *Sci. Adv.*, 2017, **3**, eaao4204.

8 H. Fu, Colloidal metal halide perovskite nanocrystals: a promising juggernaut in photovoltaic applications, *J. Mater. Chem. A*, 2019, **7**, 14357–14379.

9 A. Swarnkar, A. R. Marshall, E. M. Sanehira, B. D. Chernomordik, D. T. Moore, J. A. Christians, T. Chakrabarti and J. M. Luther, Quantum dot–induced phase stabilization of α-$CsPbI_3$ perovskite for high-efficiency photovoltaics, *Science*, 2016, **354**, 92–95.

10 M. Jeong, I. W. Choi, E. M. Go, Y. Cho, M. Kim, B. Lee, S. Jeong, Y. Jo, H. W. Choi, J. Lee, J.-H. Bae, S. K. Kwak, D. S. Kim and C. Yang, Stable perovskite solar cells with efficiency exceeding 24.8% and 0.3-V voltage loss, *Science*, 2020, **369**, 1615–1620.

11 T. Chiba and J. Kido, Lead halide perovskite quantum dots for light-emitting devices, *J. Mater. Chem. C*, 2018, **6**, 11868–11877.

12 M. Lu, Y. Zhang, S. Wang, J. Guo, W. W. Yu and A. L. Rogach, Metal Halide Perovskite Light-Emitting Devices: Promising Technology for Next-Generation Displays, *Adv. Funct. Mater.*, 2019, **29**, 1902008.

13   J. Pan, L. N. Quan, Y. Zhao, W. Peng, B. Murali, S. P. Sarmah, M. Yuan, L. Sinatra, N. M. Alyami, J. Liu, E. Yassitepe, Z. Yang, O. Voznyy, R. Comin, M. N. Hedhili, O. F. Mohammed, Z. H. Lu, D. H. Kim, E. H. Sargent and O. M. Bakr, Highly Efficient Perovskite-Quantum-Dot Light-Emitting Diodes by Surface Engineering, *Adv. Mater.*, 2016, **28**, 8718–8725.

14   H. C. Yoon, H. Lee, H. Kang, J. H. Oh and Y. R. Do, Highly efficient wide-color-gamut QD-emissive LCDs using red and green perovskite core/shell QDs, *J. Mater. Chem. C*, 2018, **6**, 13023–13033.

15   Y. Wang, L. Song, Y. Chen and W. Huang, Emerging New-Generation Photodetectors Based on Low-Dimensional Halide Perovskites, *ACS Photonics*, 2020, **7**, 10–28.

16   Q. Chen, J. Wu, X. Ou, B. Huang, J. Almutlaq, A. A. Zhumekenov, X. Guan, S. Han, L. Liang, Z. Yi, J. Li, X. Xie, Y. Wang, Y. Li, D. Fan, D. B. L. Teh, A. H. All, O. F. Mohammed, O. M. Bakr, T. Wu, M. Bettinelli, H. Yang, W. Huang and X. Liu, All-inorganic perovskite nanocrystal scintillators, *Nature*, 2018, **561**, 88–93.

17   H. Huang, M. I. Bodnarchuk, S. V. Kershaw, M. V. Kovalenko and A. L. Rogach, Lead Halide Perovskite Nanocrystals in the Research Spotlight: Stability and Defect Tolerance, *ACS Energy Lett.*, 2017, **2**, 2071–2083.

18   V. K. Ravi, P. K. Santra, N. Joshi, J. Chugh, S. K. Singh, H. Rensmo, P. Ghosh and A. Nag, Origin of the Substitution Mechanism for the Binding of Organic Ligands on the Surface of CsPbBr₃ Perovskite Nanocubes, *J. Phys. Chem. Lett.*, 2017, **8**, 4988–4994.

19   J. De Roo, M. Ibáñez, P. Geiregat, G. Nedelcu, W. Walravens, J. Maes, J. C. Martins, I. Van Driessche, M. V. Kovalenko and Z. Hens, Highly Dynamic Ligand Binding and Light Absorption Coefficient of Cesium Lead Bromide Perovskite Nanocrystals, *ACS Nano*, 2016, **10**, 2071–2081.

20   S. R. Smock, T. J. Williams and R. L. Brutchey, Quantifying the Thermodynamics of Ligand Binding to CsPbBr₃ Quantum Dots, *Angew. Chem., Int. Ed.*, 2018, **57**, 11711–11715.

21   M. I. Bodnarchuk, S. C. Boehme, S. ten Brinck, C. Bernasconi, Y. Shynkarenko, F. Krieg, R. Widmer, B. Aeschlimann, D. Günther, M. V. Kovalenko and I. Infante, Rationalizing and Controlling the Surface Structure and Electronic Passivation of Cesium Lead Halide Nanocrystals, *ACS Energy Lett.*, 2019, **4**, 63–74.

22   M. Imran, P. Ijaz, L. Goldoni, D. Maggioni, U. Petralanda, M. Prato, G. Almeida, I. Infante and L. Manna, Simultaneous Cationic and Anionic Ligand Exchange For Colloidally Stable CsPbBr₃ Nanocrystals, *ACS Energy Lett.*, 2019, **4**, 819–824.

23   Y. Dong, Y.-K. Wang, F. Yuan, A. Johnston, Y. Liu, D. Ma, M.-J. Choi, B. Chen, M. Chekini, S.-W. Baek, L. K. Sagar, J. Fan, Y. Hou, M. Wu, S. Lee, B. Sun, S. Hoogland, R. Quintero-Bermudez, H. Ebe, P. Todorovic, F. Dinic, P. Li, H. T. Kung, M. I. Saidaminov, E. Kumacheva, E. Spiecker, L.-S. Liao, O. Voznyy, Z.-H. Lu and E. H. Sargent, Bipolar-

24   J. Owen, The coordination chemistry of nanocrystal surfaces, *Science*, 2015, **347**, 615–616.

25   J. Ye, M. M. Byranvand, C. O. Martínez, R. L. Z. Hoye, M. Saliba and L. Polavarapu, Defect Passivation in Lead-Halide Perovskite Nanocrystals and Thin Films: Toward Efficient LEDs and Solar cells, *Angew. Chem., Int. Ed.*, 2021, DOI: 10.1002/anie.202102360.

26   F. Krieg, S. T. Ochsenbein, S. Yakunin, S. ten Brinck, P. Aellen, A. Süess, B. Clerc, D. Guggisberg, O. Nazarenko, Y. Shynkarenko, S. Kumar, C.-J. Shih, I. Infante and M. V. Kovalenko, Colloidal CsPbX₃ (X = Cl, Br, I) Nanocrystals 2.0: Zwitterionic Capping Ligands for Improved Durability and Stability, *ACS Energy Lett.*, 2018, **3**, 641–646.

27   F. Krieg, Q. K. Ong, M. Burian, G. Rainò, D. Naumenko, H. Amenitsch, A. Süess, M. J. Grotevent, F. Krumeich, M. I. Bodnarchuk, I. Shorubalko, F. Stellacci and M. V. Kovalenko, Stable Ultraconcentrated and Ultradilute Colloids of CsPbX₃ (X = Cl, Br) Nanocrystals Using Natural Lecithin as a Capping Ligand, *J. Am. Chem. Soc.*, 2019, **141**, 19839–19849.

28   B. Zhang, L. Goldoni, C. Lambruschini, L. Moni, M. Imran, A. Pianetti, V. Pinchetti, S. Brovelli, L. De Trizio and L. Manna, Stable and Size Tunable CsPbBr₃ Nanocrystals Synthesized with Oleylphosphonic Acid, *Nano Lett.*, 2020, **20**, 8847–8853.

29   B. Zhang, L. Goldoni, J. Zito, Z. Dang, G. Almeida, F. Zaccaria, J. de Wit, I. Infante, L. De Trizio and L. Manna, Alkyl Phosphonic Acids Deliver CsPbBr₃ Nanocrystals with High Photoluminescence Quantum Yield and Truncated Octahedron Shape, *Chem. Mater.*, 2019, **31**, 9140–9147.

30   Y. Tan, Y. Zou, L. Wu, Q. Huang, D. Yang, M. Chen, M. Ban, C. Wu, T. Wu, S. Bai, T. Song, Q. Zhang and B. Sun, Highly Luminescent and Stable Perovskite Nanocrystals with Octylphosphonic Acid as a Ligand for Efficient Light-Emitting Diodes, *ACS Appl. Mater. Interfaces*, 2018, **10**, 3784–3792.

31   D. Yang, X. Li, W. Zhou, S. Zhang, C. Meng, Y. Wu, Y. Wang and H. Zeng, CsPbBr₃ Quantum Dots 2.0: Benzenesulfonic Acid Equivalent Ligand Awakens Complete Purification, *Adv. Mater.*, 2019, **31**, 1900767.

32   B. A. Koscher, J. K. Swabeck, N. D. Bronstein and A. P. Alivisatos, Essentially Trap-Free CsPbBr₃ Colloidal Nanocrystals by Postsynthetic Thiocyanate Surface Treatment, *J. Am. Chem. Soc.*, 2017, **139**, 6566–6569.

33   D. P. Nenon, K. Pressler, J. Kang, B. A. Koscher, J. H. Olshansky, W. T. Osowiecki, M. A. Koc, L.-W. Wang and A. P. Alivisatos, Design Principles for Trap-Free CsPbX₃ Nanocrystals: Enumerating and Eliminating Surface Halide Vacancies with Softer Lewis Bases, *J. Am. Chem. Soc.*, 2018, **140**, 17760–17772.

34   T. Ahmed, S. Seth and A. Samanta, Boosting the Photoluminescence of CsPbX₃ (X = Cl, Br, I) Perovskite Nanocrystals Covering a Wide Wavelength Range by

shell resurfacing for blue LEDs based on strongly confined perovskite quantum dots, *Nat. Nanotechnol.*, 2020, **15**, 668–674.

Postsynthetic Treatment with Tetrafluoroborate Salts, *Chem. Mater.*, 2018, **30**, 3633–3637.

35 K. Hoshi, T. Chiba, J. Sato, Y. Hayashi, Y. Takahashi, H. Ebe, S. Ohisa and J. Kido, Purification of Perovskite Quantum Dots Using Low-Dielectric-Constant Washing Solvent "Diglyme" for Highly Efficient Light-Emitting Devices, *ACS Appl. Mater. Interfaces*, 2018, **10**, 24607–24612.

36 H. Wu, Y. Zhang, M. Lu, X. Zhang, C. Sun, T. Zhang, V. L. Colvin and W. W. Yu, Surface ligand modification of cesium lead bromide nanocrystals for improved light-emitting performance, *Nanoscale*, 2018, **10**, 4173–4178.

37 J. Song, J. Li, L. Xu, J. Li, F. Zhang, B. Han, Q. Shan and H. Zeng, Room-Temperature Triple-Ligand Surface Engineering Synergistically Boosts Ink Stability, Recombination Dynamics, and Charge Injection toward EQE-11.6% Perovskite QLEDs, *Adv. Mater.*, 2018, **30**, 1800764.

38 T. Chiba, K. Hoshi, Y.-J. Pu, Y. Takeda, Y. Hayashi, S. Ohisa, S. Kawata and J. Kido, High-Efficiency Perovskite Quantum-Dot Light-Emitting Devices by Effective Washing Process and Interfacial Energy Level Alignment, *ACS Appl. Mater. Interfaces*, 2017, **9**, 18054–18060.

39 J. H. Park, A.-Y. Lee, J. C. Yu, Y. S. Nam, Y. Choi, J. Park and M. H. Song, Surface Ligand Engineering for Efficient Perovskite Nanocrystal-Based Light-Emitting Diodes, *ACS Appl. Mater. Interfaces*, 2019, **11**, 8428–8435.

40 E. Moyen, H. Jun, H.-M. Kim and J. Jang, Surface Engineering of Room Temperature-Grown Inorganic Perovskite Quantum Dots for Highly Efficient Inverted Light-Emitting Diodes, *ACS Appl. Mater. Interfaces*, 2018, **10**, 42647–42656.

41 Y. S. Shin, Y. J. Yoon, K. T. Lee, J. Jeong, S. Y. Park, G.-H. Kim and J. Y. Kim, Vivid and Fully Saturated Blue Light-Emitting Diodes Based on Ligand-Modified Halide Perovskite Nanocrystals, *ACS Appl. Mater. Interfaces*, 2019, **11**, 23401–23409.

42 Y. Shynkarenko, M. I. Bodnarchuk, C. Bernasconi, Y. Berezovska, V. Verteletskyi, S. T. Ochsenbein and M. V. Kovalenko, Direct Synthesis of Quaternary Alkylammonium-Capped Perovskite Nanocrystals for Efficient Blue and Green Light-Emitting Diodes, *ACS Energy Lett.*, 2019, **4**, 2703–2711.

43 C. Zhang, B. Wang, Q. Wan, L. Kong, W. Zheng, Z. Li and L. Li, Critical role of metal ions in surface engineering toward brightly luminescent and stable cesium lead bromide perovskite quantum dots, *Nanoscale*, 2019, **11**, 2602–2607.

44 L. J. Ruan, B. Tang and Y. Ma, Improving the Stability of CsPbBr$_3$ Nanocrystals in Ethanol by Capping with PbBr2-Adlayers, *J. Phys. Chem. C*, 2019, **123**, 11959–11967.

45 J. Pan, S. P. Sarmah, B. Murali, I. Dursun, W. Peng, M. R. Parida, J. Liu, L. Sinatra, N. Alyami, C. Zhao, E. Alarousu, T. K. Ng, B. S. Ooi, O. M. Bakr and O. F. Mohammed, Air-Stable Surface-Passivated Perovskite Quantum Dots for Ultra-Robust, Single- and Two-Photon-Induced Amplified Spontaneous Emission, *J. Phys. Chem. Lett.*, 2015, **6**, 5027–5033.

46 T. Chiba, Y. Takahashi, J. Sato, S. Ishikawa, H. Ebe, K. Tamura, S. Ohisa and J. Kido, Surface Crystal Growth of Perovskite Nanocrystals via Postsynthetic Lead(II) Bromide Treatment to Increase the Colloidal Stability and Efficiency of Light-Emitting Devices, *ACS Appl. Mater. Interfaces*, 2020, **12**, 45574–45581.

47 W. Wang, X. Ji, A. Kapur, C. Zhang and H. Mattoussi, A Multifunctional Polymer Combining the Imidazole and Zwitterion Motifs as a Biocompatible Compact Coating for Quantum Dots, *J. Am. Chem. Soc.*, 2015, **137**, 14158–14172.

48 L. Du, W. Wang, C. Zhang, Z. Jin, G. Palui and H. Mattoussi, A Versatile Coordinating Ligand for Coating Semiconductor, Metal, and Metal Oxide Nanocrystals, *Chem. Mater.*, 2018, **30**, 7269–7279.

49 W. Wang, A. Kapur, X. Ji, M. Safi, G. Palui, V. Palomo, P. E. Dawson and H. Mattoussi, Photoligation of an Amphiphilic Polymer with Mixed Coordination Provides Compact and Reactive Quantum Dots, *J. Am. Chem. Soc.*, 2015, **137**, 5438–5451.

50 S. Wang, L. Du, Z. Jin, Y. Xin and H. Mattoussi, Enhanced Stabilization and Easy Phase Transfer of CsPbBr$_3$ Perovskite Quantum Dots Promoted by High-Affinity Polyzwitterionic Ligands, *J. Am. Chem. Soc.*, 2020, **142**, 12669–12680.

51 W. Wang, E. A. van Niekerk, Y. Zhang, L. Du, X. Ji, S. Wang, J. D. Baker, K. Groeniger, F. M. Raymo and H. Mattoussi, Compact, "Clickable" Quantum Dots Photoligated with Multifunctional Zwitterionic Polymers for Immunofluorescence and In Vivo Imaging, *Bioconjugate Chem.*, 2020, **31**, 1497–1509.

52 W. Wang, X. Ji, H. Bin Na, M. Safi, A. Smith, G. Palui, J. M. Perez and H. Mattoussi, Design of a Multi-Dopamine-Modified Polymer Ligand Optimally Suited for Interfacing Magnetic Nanoparticles with Biological Systems, *Langmuir*, 2014, **30**, 6197–6208.

53 J. De Roo, N. Yazdani, E. Drijvers, A. Lauria, J. Maes, J. S. Owen, I. Van Driessche, M. Niederberger, V. Wood, J. C. Martins, I. Infante and Z. Hens, Probing Solvent–Ligand Interactions in Colloidal Nanocrystals by the NMR Line Broadening, *Chem. Mater.*, 2018, **30**, 5485–5492.

54 N. C. Anderson, M. P. Hendricks, J. J. Choi and J. S. Owen, Ligand Exchange and the Stoichiometry of Metal Chalcogenide Nanocrystals: Spectroscopic Observation of Facile Metal-Carboxylate Displacement and Binding, *J. Am. Chem. Soc.*, 2013, **135**, 18536–18548.

55 W. Wang, X. Ji, L. Du and H. Mattoussi, Enhanced Colloidal Stability of Various Gold Nanostructures Using a Multicoordinating Polymer Coating, *J. Phys. Chem. C*, 2017, **121**, 22901–22913.

56 J. R. Lakowicz, *Principles of Fluorescence Spectroscopy*, Springer, US, 3rd edn, 2006.

57 C. C. Stoumpos, C. D. Malliakas, J. A. Peters, Z. Liu, M. Sebastian, J. Im, T. C. Chasapis, A. C. Wibowo, D. Y. Chung, A. J. Freeman, B. W. Wessels and M. G. Kanatzidis,

Crystal Growth of the Perovskite Semiconductor CsPbBr3: A New Material for High-Energy Radiation Detection, *Cryst. Growth Des.*, 2013, **13**, 2722–2727.

58 F. Bertolotti, L. Protesescu, M. V. Kovalenko, S. Yakunin, A. Cervellino, S. J. L. Billinge, M. W. Terban, J. S. Pedersen, N. Masciocchi and A. Guagliardi, Coherent Nanotwins and Dynamic Disorder in Cesium Lead Halide Perovskite Nanocrystals, *ACS Nano*, 2017, **11**, 3819–3831.

59 P. Cottingham and R. L. Brutchey, On the crystal structure of colloidally prepared CsPbBr$_3$ quantum dots, *Chem. Commun.*, 2016, **52**, 5246–5249.

60 Z.-J. Li, E. Hofman, J. Li, A. H. Davis, C.-H. Tung, L.-Z. Wu and W. Zheng, Photoelectrochemically Active and Environmentally Stable CsPbBr$_3$/TiO2 Core/Shell Nanocrystals, *Adv. Funct. Mater.*, 2018, **28**, 1704288.

61 Y. Xia, X. Xia and H.-C. Peng, Shape-Controlled Synthesis of Colloidal Metal Nanocrystals: Thermodynamic versus Kinetic Products, *J. Am. Chem. Soc.*, 2015, **137**, 7947–7966.

62 Q. Zhong, M. Cao, Y. Xu, P. Li, Y. Zhang, H. Hu, D. Yang, Y. Xu, L. Wang, Y. Li, X. Zhang and Q. Zhang, L-Type Ligand-Assisted Acid-Free Synthesis of CsPbBr3 Nanocrystals with Near-Unity Photoluminescence Quantum Yield and High Stability, *Nano Lett.*, 2019, **19**, 4151–4157.

63 J. Kirchnerová and G. C. B. Cave, The solubility of water in low-dielectric solvents, *Can. J. Chem.*, 1976, **54**, 3909–3916.

64 B. T. Mai, M. J. Barthel, A. Lak, T. Avellini, A. M. Panaite, E. M. Rodrigues, L. Goldoni and T. Pellegrino, Photo-induced copper mediated copolymerization of activated-ester methacrylate polymers and their use as reactive pre-cursors to prepare multi-dentate ligands for the water transfer of inorganic nanoparticles, *Polym. Chem.*, 2020, **11**, 2969–2985.

65 K. Malhotra, R. Fuku, T. S. Chan, N. Kraljevic, A. Sedighi, P. A. E. Piunno and U. J. Krull, Bisphosphonate Polymeric Ligands on Inorganic Nanoparticles, *Chem. Mater.*, 2020, **32**, 4002–4012.

66 E. Giovanelli, E. Muro, G. Sitbon, M. Hanafi, T. Pons, B. Dubertret and N. Lequeux, Highly Enhanced Affinity of Multidentate versus Bidentate Zwitterionic Ligands for Long-Term Quantum Dot Bioimaging, *Langmuir*, 2012, **28**, 15177–15184.

67 A. Stelmakh, M. Aebli, A. Baumketner and M. V. Kovalenko, On the Mechanism of Alkylammonium Ligands Binding to the Surface of CsPbBr3 Nanocrystals, *Chem. Mater.*, 2021, **33**, 5962–5973.

68 H. Kim, N. Hight-Huf, J.-H. Kang, P. Bisnoff, S. Sundararajan, T. Thompson, M. Barnes, R. C. Hayward and T. Emrick, Polymer Zwitterions for Stabilization of CsPbBr$_3$ Perovskite Nanoparticles and Nanocomposite Films, *Angew. Chem., Int. Ed.*, 2020, **59**, 10802–10806.

69 T. A. Cohen, Y. Huang, N. A. Bricker, C. S. Juhl, T. J. Milstein, J. D. MacKenzie, C. K. Luscombe and D. R. Gamelin, Modular Zwitterion-Functionalized Poly(iso-propyl methacrylate) Polymers for Hosting Luminescent Lead Halide Perovskite Nanocrystals, *Chem. Mater.*, 2021, **33**, 3779–3790.

70 A. Dey, J. Ye, A. De, E. Debroye, S. K. Ha, E. Bladt, A. S. Kshirsagar, Z. Wang, J. Yin, Y. Wang, L. N. Quan, F. Yan, M. Gao, X. Li, J. Shamsi, T. Debnath, M. Cao, M. A. Scheel, S. Kumar, J. A. Steele, M. Gerhard, L. Chouhan, K. Xu, X.-G. Wu, Y. Li, Y. Zhang, A. Dutta, C. Han, I. Vincon, A. L. Rogach, A. Nag, A. Samanta, B. A. Korgel, C.-J. Shih, D. R. Gamelin, D. H. Son, H. Zeng, H. Zhong, H. Sun, H. V. Demir, I. G. Scheblykin, I. Mora-Seró, J. K. Stolarczyk, J. Z. Zhang, J. Feldmann, J. Hofkens, J. M. Luther, J. Pérez-Prieto, L. Li, L. Manna, M. I. Bodnarchuk, M. V. Kovalenko, M. B. J. Roeffaers, N. Pradhan, O. F. Mohammed, O. M. Bakr, P. Yang, P. Müller-Buschbaum, P. V. Kamat, Q. Bao, Q. Zhang, R. Krahne, R. E. Galian, S. D. Stranks, S. Bals, V. Biju, W. A. Tisdale, Y. Yan, R. L. Z. Hoye and L. Polavarapu, State of the Art and Prospects for Halide Perovskite Nanocrystals, *ACS Nano*, 2021, **15**, 10775–10981.